2.5. Mice Treated with Memantine and AMPA Were Unable to Walk Smoothly

GRID2 deficiency results in dysregulation of AMPA receptors [34,35]. To examine whether impaired AMPA receptor functions affected memantine susceptibility, mice were treated with memantine simultaneously with the AMPA receptor agonist AMPA or the antagonist DNQX [36], and the movements of these mice were monitored (Figure 5A). The mice treated with AMPA (20 mg/kg) walked slowly and sometimes crouched on the floor. However, mice treated with both memantine (10 mg/kg) and AMPA had increased activity and did not stop walking. In addition to these abnormal behaviors, the mice walked with a mild staggering gait and sometimes slipped (roll-over: Figure 5B, Supplementary Movie 4). These combined effects of memantine on mouse behavior were not observed when memantine was administered with DNQX (10 mg/kg), although the mice treated with DNQX were also sometimes crouched. Moreover, in the *Grid2*$^{Htake/Htake}$ mice, co-treatment with AMPA and a low dose of memantine (5 mg/kg) caused more evident balance impairment than memantine treatment alone (Supplementary Figure S3), suggesting that GRID2 deficiency may augment the synergistic action of AMPA and memantine. The effect of AMPA co-treatment could not be evaluated with a higher dose of memantine (10 mg/kg) because the maximal effect was induced by this dose of memantine.

Figure 5. Effect of AMPA receptor modulators on memantine action in WT mice. (**A**) Monitoring of walking mice (12-week-old WT male, n = 6) after memantine treatment (10 mg/kg) combined with AMPA (20 mg/kg) or the AMPA receptor antagonist DNQX (10 mg/kg). Ten minutes after the treatments, the walking distance for 5 min was expressed as the mean and SD, * $p < 0.05$ *vs.* the other conditions (unpaired *t*-test; $p < 0.0001$ for overall differences, one-way ANOVA); (**B**) Number of rollovers in 5 min was counted. NO indicates that rollover was not observed. n = 6 for Control and AMPA + memantine and n = 3 for the other conditions. The occurrence of rollover was significantly different between AMPA + memantine and the other conditions ($p < 0.05$, Fisher's exact test); (**C**) OKRs measured in female WT mice with sequential injections of the control saline, AMPA (10 mg/kg), or DNQX (5 mg/kg) and memantine (5 mg/kg). A set of traces indicates representative responses of individual mice. Dotted line, the movement of the stimulus screen; (**D**) Graph shows the mean and ±SD of OKR gain (n = 3 for each condition). *p* value (without a bracket, one-tailed unpaired *t*-test; with brackets, paired *t*-test) is indicated when significance was observed.

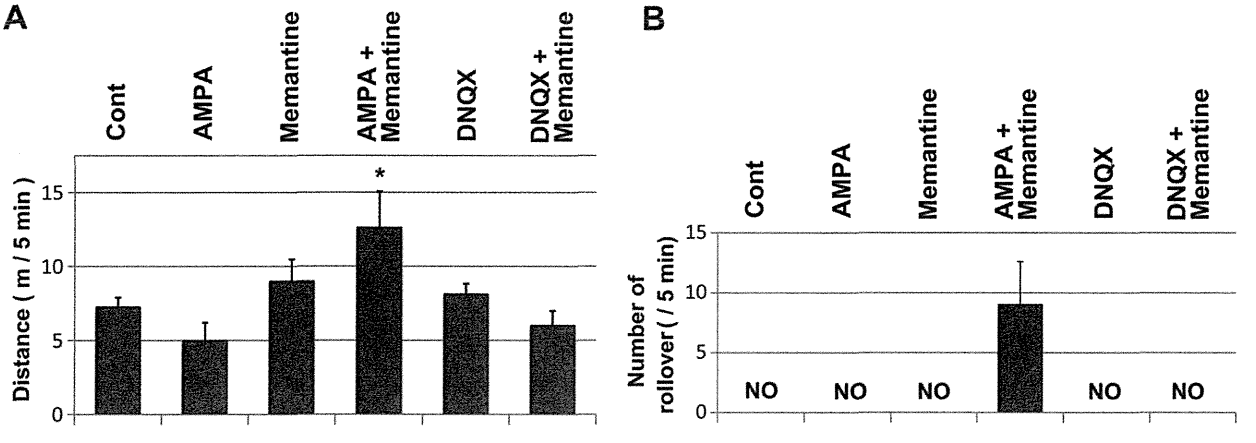

Figure 5. *Cont.*

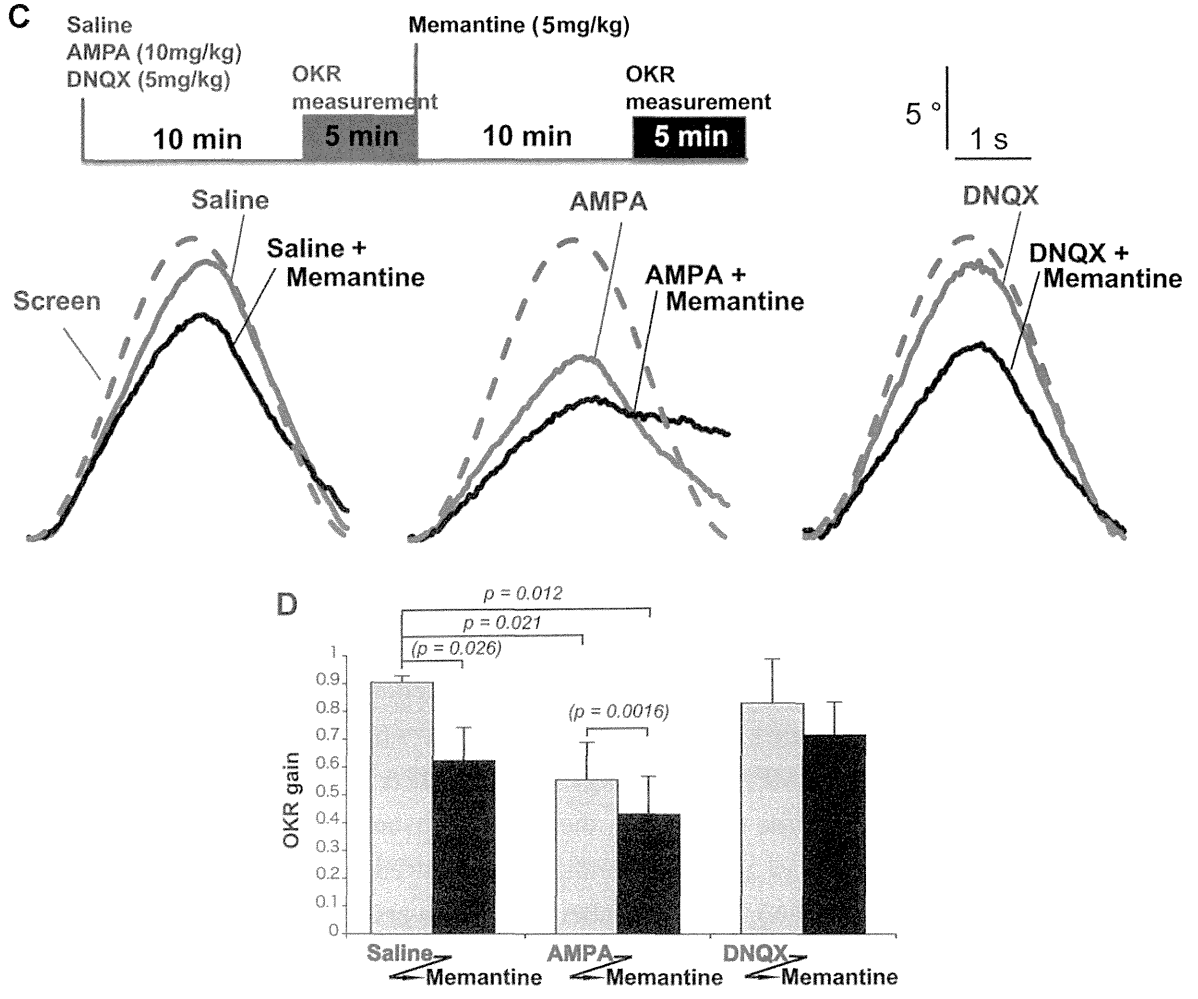

Finally, the OKR was monitored after co-treatment with memantine and AMPA or DNQX (Figure 5C). Mice were first treated with AMPA, DNQX, or saline, and the OKR was subsequently monitored for 5 min (because some mice closed their eyes after treatment with higher doses, AMPA (10 mg/kg) and DNQX (5 m/kg) were used for OKR measurement). To evaluate synergies between memantine and AMPA receptor modulators, the mice were further treated with a low dose of memantine (5 mg/kg), and again subjected to OKR measurements for another 5 min. AMPA significantly impaired the OKR, and the combined treatment with memantine further impaired the OKR (Figure 5D). These effects were not observed in mice co-treated with memantine and DNQX.

3. Discussion

Here, we report cross-talk between GRID2 signaling and memantine in mice, which may, in part, account for the adverse effects of memantine in patients with individual differences in congenital or acquired genetic factors, such as GRID2.

Major phenotypes have been identified in GRID2 mutant mice, including impaired motor coordination, learning, and memory. GRID2 is located on the postsynaptic membrane of Purkinje cells and binds to cerebellin precursor protein 1 (CBLN1) and neurexin 1 beta (NRXN1b) [7,8] on the parallel fibers of granule cells [7,37]. On the other hand, the memantine target, NMDA receptors, are also

expressed on the developing [38] and adult [39] cerebellar granule cells. Furthermore, contrary to the neurotoxic effects of glutamate, NMDA receptors were found to promote the survival of cultured Purkinje [40] and granule cells [41,42]. However, double-KO mice with disrupted *Nr2A* and *Nr2C* genes (encoding two major NMDA receptor subunits in the adult mice cerebellum) demonstrate a mild impairment in motor coordination, but they do not exhibit an ataxic phenotype [43]. This observation suggests that NMDA receptors and GRID2 functions may not be directly linked [44].

Thus, in the present study, pharmaco-behavioral approaches failed to identify *Grid2* as a candidate for the cause of the observed phenotypes. Unexpectedly, our efforts resulted in the observation of new phenotypes in our *Grid2* deficient mice, which appeared as enhanced memantine susceptibility, which was likely mediated by dysfunctional NMDA receptors [1,2,45]. OKR measurements in $Grid2^{Htake/Htake}$ mice revealed impaired basal cerebellar functions in eye movement, which was also mimicked by memantine treatment. Dizziness has been reported as a major adverse effect of memantine treatment in humans [6,46]. The cerebellar flocculus is thought to be responsible for the early stage formation of OKR adaptation and its memory [47,48].

The *Grid2* gene is located in a hot spot of genomic deletions [31], and a number of mutant lines with defects in this gene have been identified. In addition to naturally occurring mutants, targeted disruption and knock-in mutations of *Grid2* have been reported [30,49,50]. In contrast to these loss-of-function mutations, $Grid2^{Lc}$ (*Lurcher*) [51] was identified as a spontaneous dominant mutation characterized by cerebellar ataxia and atrophy of Purkinje and granule cells [30]. Physiological studies of $Grid2^{Lc/+}$ mice have shown that the $Grid2^{Lc}$ mutation produces constitutive inward Ca^{2+}/Na^{+} currents that induce cell death [52].

The importance of the genetic background on $Grid2^{Lc/+}$ mice phenotypes was also reported [47,53]. In congenic $Grid2^{Lc/+}$ mice, almost 99.99% of those on a C57BL/6 genetic background lost Purkinje cells, whereas no Purkinje cell loss was observed in $Grid2^{Lc/+}$ mice on a 93% C57BL/6 genetic background, indicating that phenotypes in $Grid2^{Lc/+}$ mice are highly dependent on their genetic backgrounds. Interestingly, abnormal eye-movement and impaired motor-coordination were only observed in 93% of C57BL/6 background-$Grid2^{Lc/+}$ mice possessing Purkinje cells, but not in 99.99% of C57BL/6 background-$Grid2^{Lc/+}$ mice without Purkinje cells [47], suggesting that gain of GRID2 signaling is also a cause of motor deficits in the presence of Purkinje cells. In contrast to $Grid2^{Lc/+}$ mice, we noticed during gene mapping that memantine-induced balance impairment was observed in $Grid2^{Htake/Htake}$ mice irrespective of their genetic backgrounds (mixed B6 and C3 backgrounds). This is also the case for random eye movements commonly observed in different *Grid2*-deleted mice with different genetic backgrounds, *Grid2*-KO in C57BL/6 and $Grid2^{ho\text{-}15J/15J}$ on a C3HJ background [17], suggested that memantine-induced balance impairment may occur in other *Grid2* deficient mice irrespective of their genetic backgrounds.

How does the $Grid2^{Htake}$ deletion enhance the actions of memantine? GRID2 regulates long-term depression (LTD) at synapses between immature parallel fibers and Purkinje cells by inducing AMPA receptor endocytosis [34,35]. D-Serine is an endogenous ligand for GRID2 and one of the factors that induce LTD [9]. Developing mice that express GRID2 with a disrupted D-serine binding site show impaired motor coordination and learning, suggesting the importance of LTD for motor regulation. On the other hand, NMDA receptor activation requires the removal of Mg^{2+} block, which occurs when the membrane potential increases through activation of non-NMDA receptors including AMPA receptors [4].

Cooperative signal-transmission from cerebellar mossy fiber-granule cells to Purkinje cells mediated by NMDA and AMPA receptors has been shown in both Mg^{2+} block dependent and independent manners [54]. We observed that co-treatment with memantine and AMPA impaired gait and OKR in wild type mice, suggesting that dysregulation of AMPA receptor function in *Grid2* deficient mice may cause the enhanced memantine susceptibility. This may be implicated in the decreased number of memantine-sensitive NMDA-responsible granule cells in *Grid2*$^{Htake/Htake}$ mice.

Whilst mapping the gene responsible for the ataxic phenotype, we observed new phenotypes in *Grid2* deficient mice, which were latent balance defects, and OKR impairments. These deficits were also mimicked by memantine with AMPA in the impaired WT mice. Because, recently, the wide distributions of *Grid2* mRNA and GRID2 protein were reported in the adult rodent brain [55], the phenotypes in *Grid2*$^{Htake/Htake}$ mice could be ascribed to not only attenuated NMDA receptor responsiveness in a subset of granule cells but also other cellular mechanisms.

When granule cells are collectively activated *in vivo*, glutamate spilt over from parallel fiber-Purkinje cell synapses stimulate adjacent interneurons (volume transmission), which in turn exert inhibition of Purkinje cells [44,56–58] crucial for normal motor coordination [59]. The GRID2 mutation may reduce NMDA receptor-mediated excitation of granule cells, and this might decrease the volume transmission and Purkinje cell inhibition via interneurons. Moreover, cerebellar interneurons (basket, stellate, and Golgi cells) also express functional NMDA receptors at their presynaptic membrane [44,56–58] and these receptors could be affected by the change of GRID2 signaling. Taken as a whole, the present study using a naturally occurring *Grid2* deleted mouse line may lead to a better understanding of NMDA, AMPA, and GRID2 receptors. Further studies are required to elucidate the precise mechanisms underlying GRID2 signaling.

4. Experimental Section

4.1. Animals

C57BL/6J (B6) and C3H/HeN (C3) from SLC Japan (Shizuoka, JAPAN) were used for the maintenance of the *Grid2*$^{Htake/Htake}$ mouse line and for IVF for microsatellite analyses, respectively. IVF was performed following a standard method [60] using human tubal fluid medium (Ark Resource, Kumamoto, Japan). The *Grid2* mutant mice, *Grid2*$^{Htake/Htake}$ (formal name is *Grid2*$^{ho\text{-}Htake}$/Nibio), were supplied by the JCRB Laboratory Animal Resource Bank at the National Institute of Biomedical Innovation. The experimental mouse protocols were approved by the Ethics Committee at the National Institute of Biomedical Innovation (assigned No. DS-23-35), and by the University of Toyama's Committee on Animal Experiments (assigned No. A2012eng-8) for animal welfare. For microarray analyses, cerebella were dissected after anesthesia of mice with isoflurane (WAKO Pure Chemicals, Osaka, JAPAN). The animals were maintained under standard light (08:00–20:00) and temperature conditions (23 °C, 50% humidity).

4.2. Reagents

Microsatellite markers were used to identify the chromosomal region responsible for the ataxic phenotype, (D6Mit86, 1.18 cM; D6Mit351, 22.94 cM; D6Mit384, 27.38 cM; D6Mit243, 32.2 cM 7;

D6Mit29, 37.75 cM; D6Mit102. 42.11 cM; D6Mit149, 48.93 cM; D6Mit200, 89.28 cM). To map the end points of the *Grid2* deletion, we used following primers: m*Grid2* intron 2H F 5'-GCT ACT TTG GTA CAA GTG GAC A and m*Grid2* intron 2H R 5'-GAC AAG TTG CTC TCT GTA TCT; m*Grid2* Intron 2I F 5'-CAT GCT CAC ATC AAA ATA CAT CAA and m*Grid2* Intron 2I R 5'-TGT AAT TGA GGAA AAT ACA TAA T. Other primers used in Figure 3D were prepared with reference to [31]. To identify the *Grid2* deletion in *Grid2*$^{Htake/Htake}$ mice, we used the following primers for PCR amplification: m*Grid2* Intron 2HIF 5'-TGG ATC CTT CTA CGT GCA AC, m*Grid2* Intron 8YF2 5'-GGA CCA CAC TGA GGT TCG AAA GA, and m*Grid2* Intron 8YR 5'-ATC TCT TGG CAT GCA TTA GAC. The mutant allele of *Grid2*^{Htake} produces a PCR band corresponding to a product of approximately 600 bp, and that for the WT allele is approximately 400 bp.

GRID2 antibody was obtained from Santa Cruz Biotechnology (Santa Cruz, CA, USA). Antibodies for NMDAR1 and tubulin were obtained from Cell Signaling Technology (Boston, MA, USA). Memantine, AMPA, DNQX, MK-801, nitrazepam, donepezil, and ondansetron were purchased from WAKO Pure Chemicals; ifenprodil, Ro25-6981, DL-AP7, felbamate, and loperamide were obtained from Sigma-Aldrich (St. Louis, MO, USA).

4.3. mRNA Analyses

Total RNA was prepared from the cerebellar hemispheres of 12-week-old mice (male and female) using the EZ1-RNA purification kit (Qiagen, Venlo Park, The Netherlands). For microarray analyses, GeneChip Mouse Genome 430A (Affymetrix, Santa Clara, CA, USA) was used, and differences in transcript levels were calculated with Partek (Partek Inc., St. Louis, MO, USA). The original data files (CEL-files) were deposited in the Gene Expression Omnibus (GEO) repository and assigned the GEO accession numbers: GSM1334015, GSM1334016, and GSM1334017 for normal mice, and GSM1334018, GSM1334019, and GSM1334020 for mutant mice. PCR primers for real-time PCR were as follows: *mGrid2* F, 5'-AAC ACG CTA CAT GGA CTA CTC-3' and *mGrid2* R, 5'-GAA GCA CTG TGC CAG CAA TG-3'; m*Gapdh* F, 5'-ACT CAC GGC AAA TTC AAC GG-3' and m*Gapdh* R, 5'-GAC TCC ACG ACA TAC TGA GC-3'. To amplify the *Grid2* ORF, primers are mGrid2 F2 (5ATG): 5'-ATG GAA GTT TTC CCC TTG CTC TTG T and mGrid2 R (3Stop): 5'-TCA TAT GGA CGT GCC TCG GTC GGG GTC A were used.

4.4. Measurements of Walking Distance and the OKR

Male mice (12–14 weeks old) were placed in a rectangular box (25 cm × 40 cm), and their head position was tracked for 5 min using ANY-maze software (Brain Science Idea, Osaka, Japan). Each mouse was monitored three times, and the longest distance recorded was used in the data analysis.

The OKR was measured in adult mice using previously described methods [28], which are depicted in Supplementary Figure S1. Briefly, the mice were anesthetized with isoflurane (2%) and a stainless steel screw was glued to the skull. The mice were then habituated to the experimental conditions for 2 days before the measurement. Ten minutes before the measurement were made, mice were administered a saline (8 mL/kg) injection with or without memantine (10 mg/kg) intraperitoneally. The mouse was then mounted on a stereotaxic apparatus and exposed to continuous sinusoidal horizontal oscillations (17°, 0.25 Hz) of a cylindrical checkerboard-patterned screen (diameter, 65 cm; single

square, 1.8 × 1.8 cm; brightness, ~30 lx). Right eye movement was captured at 30 Hz with an infrared camera. For each image frame, we used a machine vision system to estimate the pupil azimuth from the location of the pupil center. The OKR was expressed on a time plot of the relative pupil azimuth for each round of screen oscillation, with the pupil azimuth at the beginning of backward eye movement set to 0°. An OKR gain was defined as the ratio of the maximal relative pupil azimuth change to that of the screen (17°).

4.5. Cell Culture and Electrophysiology

Granule cell-enriched cultures were prepared as previously described [61]. Briefly, 2-day-old (P2) mutant or WT mice were anesthetized by cooling and then sacrificed by decapitation. The cerebella were dissociated with trypsin, plated on poly-L-ornithine-coated plastic dishes (Becton Dickinson, Franklin Lakes, NJ, USA) at 1.25 million cells/mL, and maintained in low-serum, nutrient-supplemented Dulbecco's Modified Eagle Medium/F-12 (Life Technologies; 5% CO_2, 37 °C) for 12 days.

Ruptured-patch whole-cell recordings were performed on cultured granule cells. The pipette solution contained 134 mM potassium D-gluconic acid, 7.6 mM KCl, 9 mM KOH, 10 mM NaCl, 1.2 mM $MgCl_2$, 4 mM ATP magnesium salt, 10 mM HEPES, and 0.5 mM EGTA (pH 7.3). The culture dish was perfused at a rate of 1.4 mL/min with 145 mM NaCl, 5 mM KCl, 2 mM $CaCl_2$, 10 mM HEPES, 10 mM D-glucose, and 10 μM glycine (pH 7.4). Current signals were recorded using an EPC-8 amplifier (holding potential, −90 mV; cut-off frequency, 5 kHz; sampling rate, 20 kHz; HEKA, Lambrecht/Pfalz, Germany) controlled by Patchmaster software (version, 2.35; HEKA). The command potentials were corrected for a liquid junction potential between the pipette and bath solutions. Electronic capacitance cancellation and series resistance compensation were not used. The series resistance (33.2 ± 5.1 MΩ, n = 55) and membrane capacitance were estimated from the amplitude and time constant of the capacitive current evoked by a 10 mV voltage jump. The bath solution containing 20 μM NMDA or 10 μM memantine was locally applied to the cell through a theta tube under the control of gravity and electromagnetic valves (VM8, ALA Scientific Instruments, Farmingdale, NY, USA). The magnitude of an NMDA-induced current was quantified as the inward current charge over a 2 s NMDA application normalized to the membrane capacitance (charge density). The background charge was estimated from a 0.5 s pre-application period and subtracted from the charge density.

4.6. Statistical Analyses

Data from each group were characterized by the mean ± SD, unless otherwise stated. Data from biochemical assays were examined with one-way ANOVA followed by unpaired two-tailed *t*-tests to detect statistically significant differences. All the statistical examinations were performed using JMP software (versions 9.0.2 and 10.0.1, SAS Institute, Cary, NC, USA).

Acknowledgments

We thank Junko Morita for her technical assistance and Takayoshi Imazawa for their kind advice. We thank Sebnem Kesaf and Ryuichi Shigemoto for their advice on performing OKR measurements.

This study was supported by Grants-in-Aid for Scientific Research from the Ministry of Education, Culture, Sports, Science, and Technology, Japan (25670155, 23500384, 23500384); the grant from the Ministry of Health, Labor, and Welfare (2013–2017, 2014–2016); Scientific Research on Innovative Areas, a MEXT Grant-in-Aid Project 2012–2013; Strategic Research Foundation at Private Universities (2013–2017); the grant from the Human Science Foundation (2012–2013); and a grant from the Uehara Memorial Foundation.

Author Contributions

A.K., A.F., T.Y., Y.N., Y.H., T.S., Y.I., M.K., O.S., S.A, H.R., A.K., L.P.T, M.S., T.F., H.T. performed experiments. K.K., Y.N., H.K., K.M., T.N., J.M. T.T., H.T. analyzed data. T.T., H.T. wrote the manuscript.

Conflicts of Interest

No conflicts of interest, financial or otherwise, are declared by the author(s).

References

1. Sonkusare, S.K.; Kaul, C.L.; Ramarao, P. Dementia of Alzheimer's disease and other neurodegenerative disorders—Memantine, a new hope. *Pharmacol. Res.* **2005**, *51*, 1–17.
2. Lipton, S.A. Paradigm shift in neuroprotection by NMDA receptor blockade: Memantine and beyond. *Nat. Rev. Drug Discov.* **2006**, *5*, 160–170.
3. Szczurowska, E.; Mares, P. NMDA and AMPA receptors: Development and status epilepticus. *Physiol. Res.* **2013**, *62* (Suppl. 1), S21–S38.
4. Kupper, J.; Ascher, P.; Neyton, J. Probing the pore region of recombinant N-methyl-D-aspartate channels using external and internal magnesium block. *Proc. Natl. Acad. Sci. USA* **1996**, *93*, 8648–8653.
5. Wong, E.H.; Kemp, J.A.; Priestley, T.; Knight, A.R.; Woodruff, G.N.; Iversen, L.L. The anticonvulsant MK-801 is a potent N-methyl-D-aspartate antagonist. *Proc. Natl. Acad. Sci. USA* **1986**, *83*, 7104–7108.
6. Hansen, R.A.; Gartlehner, G.; Lohr, K.N.; Kaufer, D.I. Functional outcomes of drug treatment in Alzheimer's disease: A systematic review and meta-analysis. *Drugs Aging* **2007**, *24*, 155–167.
7. Uemura, T.; Lee, S.J.; Yasumura, M.; Takeuchi, T.; Yoshida, T.; Ra, M.; Taguchi, R.; Sakimura, K.; Mishina, M. Trans-synaptic interaction of GluRdelta2 and Neurexin through Cbln1 mediates synapse formation in the cerebellum. *Cell* **2010**, *141*, 1068–1079.
8. Matsuda, K.; Miura, E.; Miyazaki, T.; Kakegawa, W.; Emi, K.; Narumi, S.; Fukazawa, Y.; Ito-Ishida, A.; Kondo, T.; Shigemoto, R.; *et al.* Cbln1 is a ligand for an orphan glutamate receptor delta2, a bidirectional synapse organizer. *Science* **2010**, *328*, 363–368.
9. Kakegawa, W.; Miyoshi, Y.; Hamase, K.; Matsuda, S.; Matsuda, K.; Kohda, K.; Emi, K.; Motohashi, J.; Konno, R.; Zaitsu, K.; *et al.* D-Serine regulates cerebellar LTD and motor coordination through the delta2 glutamate receptor. *Nat. Neurosci.* **2011**, *14*, 603–611.

10. Jardon, B.; Bonaventure, N. N-Methyl-D-aspartate antagonists suppress the development of frog symmetric monocular optokynetic nystagmus observed after unilateral visual deprivation. *Brain Res. Dev. Brain Res.* **1992**, *67*, 67–73.
11. Godaux, E.; Cheron, G.; Mettens, P. Ketamine induces failure of the oculomotor neural integrator in the cat. *Neurosci. Lett.* **1990**, *116*, 162–167.
12. Mettens, P.; Cheron, G.; Godaux, E. NMDA receptors are involved in temporal integration in the oculomotor system of the cat. *Neuroreport* **1994**, *5*, 1333–1336.
13. Huang, Y.J.; Lin, C.H.; Lane, H.Y.; Tsai, G.E. NMDA Neurotransmission Dysfunction in Behavioral and Psychological Symptoms of Alzheimer's Disease. *Curr. Neuropharmacol.* **2012**, *10*, 272–285.
14. Puangthong, U.; Hsiung, G.Y. Critical appraisal of the long-term impact of memantine in treatment of moderate to severe Alzheimer's disease. *Neuropsychiatr. Dis. Treat.* **2009**, *5*, 553–561.
15. Utine, G.E.; Haliloglu, G.; Salanci, B.; Cetinkaya, A.; Kiper, P.O.; Alanay, Y.; Aktas, D.; Boduroglu, K.; Alikasifoglu, M. A Homozygous Deletion in GRID2 Causes a Human Phenotype With Cerebellar Ataxia and Atrophy. *J. Child Neurol.* **2013**, *28*, 926–932.
16. Maier, A.; Klopocki, E.; Horn, D.; Tzschach, A.; Holm, T.; Meyer, R.; Meyer, T. *De novo* partial deletion in GRID2 presenting with complicated spastic paraplegia. *Muscle Nerve* **2014**, *49*, 289–292.
17. Hills, L.B.; Masri, A.; Konno, K.; Kakegawa, W.; Lam, A.T.; Lim-Melia, E.; Chandy, N.; Hill, R.S.; Partlow, J.N.; Al-Saffar, M.; *et al.* Deletions in GRID2 lead to a recessive syndrome of cerebellar ataxia and tonic upgaze in humans. *Neurology* **2013**, *81*, 1378–1386.
18. Van Schil, K.; Meire, F.; Karlstetter, M.; Bauwens, M.; Verdin, H.; Coppieters, F.; Scheiffert, E.; van Nechel, C.; Langmann, T.; Deconinck, N.; *et al.* Early-onset autosomal recessive cerebellar ataxia associated with retinal dystrophy: New human hotfoot phenotype caused by homozygous GRID2 deletion. *Genet. Med.* **2014**, doi:10.1038/gim.2014.95.
19. Uebi, T.; Itoh, Y.; Hatano, O.; Kumagai, A.; Sanosaka, M.; Sasaki, T.; Sasagawa, S.; Doi, J.; Tatsumi, K.; Mitamura, K.; *et al.* Involvement of SIK3 in glucose and lipid homeostasis in mice. *PLOS ONE* **2012**, *7*, e37803.
20. Hemmings, H.C., Jr.; Yan, W.; Westphalen, R.I.; Ryan, T.A. The general anesthetic isoflurane depresses synaptic vesicle exocytosis. *Mol. Pharmacol.* **2005**, *67*, 1591–1599.
21. Rammes, G.; Danysz, W.; Parsons, C.G. Pharmacodynamics of memantine: An update. *Curr. Neuropharmacol.* **2008**, *6*, 55–78.
22. Seeman, P.; Caruso, C.; Lasaga, M. Memantine agonist action at dopamine D2High receptors. *Synapse* **2008**, *62*, 149–153.
23. Lee, J.W.; Park, H.J.; Choi, J.; Park, S.J.; Kang, H.; Kim, E.G. Comparison of ramosetron's and ondansetron's preventive anti-emetic effects in highly susceptible patients undergoing abdominal hysterectomy. *Korean J. Anesthesiol.* **2011**, *61*, 488–492.
24. Khojasteh, A.; Sartiano, G.; Tapazoglou, E.; Lester, E.; Gandara, D.; Bernard, S.; Finn, A. Ondansetron for the prevention of emesis induced by high-dose cisplatin. A multi-center dose-response study. *Cancer* **1990**, *66*, 1101–1105.
25. Jayadev, S.; Bird, T.D. Hereditary ataxias: Overview. *Genet. Med.* **2013**, *15*, 673–683.

26. Requena, T.; Espinosa-Sanchez, J.M.; Lopez-Escamez, J.A. Genetics of dizziness: Cerebellar and vestibular disorders. *Curr. Opin. Neurol.* **2014**, *27*, 98–104.
27. Rosini, F.; Federighi, P.; Pretegiani, E.; Piu, P.; Leigh, R.J.; Serra, A.; Federico, A.; Rufa, A. Ocular-motor profile and effects of memantine in a familial form of adult cerebellar ataxia with slow saccades and square wave saccadic intrusions. *PLOS ONE* **2013**, *8*, e69522.
28. Shirai, Y.; Asano, K.; Takegoshi, Y.; Uchiyama, S.; Nonobe, Y.; Tabata, T. A simple machine vision-driven system for measuring optokinetic reflex in small animals. *J. Physiol. Sci.* **2013**, *63*, 395–399.
29. Shutoh, F.; Ohki, M.; Kitazawa, H.; Itohara, S.; Nagao, S. Memory trace of motor learning shifts transsynaptically from cerebellar cortex to nuclei for consolidation. *Neuroscience* **2006**, *139*, 767–777.
30. Zuo, J.; de Jager, P.L.; Takahashi, K.A.; Jiang, W.; Linden, D.J.; Heintz, N. Neurodegeneration in Lurcher mice caused by mutation in delta2 glutamate receptor gene. *Nature* **1997**, *388*, 769–773.
31. Wang, Y.; Matsuda, S.; Drews, V.; Torashima, T.; Meisler, M.H.; Yuzaki, M. A hot spot for hotfoot mutations in the gene encoding the delta2 glutamate receptor. *Eur. J. Neurosci.* **2003**, *17*, 1581–1590.
32. Cull-Candy, S.G.; Wyllie, D.J. Glutamate-receptor channels in mammalian glial cells. *Ann. N. Y. Acad. Sci.* **1991**, *633*, 458–474.
33. Kato, A.S.; Knierman, M.D.; Siuda, E.R.; Isaac, J.T.; Nisenbaum, E.S.; Bredt, D.S. Glutamate receptor delta2 associates with metabotropic glutamate receptor 1 (mGluR1), protein kinase Cgamma, and canonical transient receptor potential 3 and regulates mGluR1-mediated synaptic transmission in cerebellar Purkinje neurons. *J. Neurosci.* **2012**, *32*, 15296–15308.
34. Hirai, H.; Launey, T.; Mikawa, S.; Torashima, T.; Yanagihara, D.; Kasaura, T.; Miyamoto, A.; Yuzaki, M. New role of delta2-glutamate receptors in AMPA receptor trafficking and cerebellar function. *Nat. Neurosci.* **2003**, *6*, 869–876.
35. Yamasaki, M.; Miyazaki, T.; Azechi, H.; Abe, M.; Natsume, R.; Hagiwara, T.; Aiba, A.; Mishina, M.; Sakimura, K.; Watanabe, M. Glutamate receptor delta2 is essential for input pathway-dependent regulation of synaptic AMPAR contents in cerebellar Purkinje cells. *J. Neurosci.* **2011**, *31*, 3362–3374.
36. Honore, T.; Davies, S.N.; Drejer, J.; Fletcher, E.J.; Jacobsen, P.; Lodge, D.; Nielsen, F.E. Quinoxalinediones: Potent competitive non-NMDA glutamate receptor antagonists. *Science* **1988**, *241*, 701–703.
37. Kakegawa, W.; Miyazaki, T.; Kohda, K.; Matsuda, K.; Emi, K.; Motohashi, J.; Watanabe, M.; Yuzaki, M. The N-terminal domain of GluD2 (GluRdelta2) recruits presynaptic terminals and regulates synaptogenesis in the cerebellum *in vivo*. *J. Neurosci.* **2009**, *29*, 5738–5748.
38. Rabacchi, S.; Bailly, Y.; Delhaye-Bouchaud, N.; Mariani, J. Involvement of the N-methyl D-aspartate (NMDA) receptor in synapse elimination during cerebellar development. *Science* **1992**, *256*, 1823–1825.
39. Garthwaite, J.; Brodbelt, A.R. Synaptic activation of N-methyl-D-aspartate and non-N-methyl-D-aspartate receptors in the mossy fibre pathway in adult and immature rat cerebellar slices. *Neuroscience* **1989**, *29*, 401–412.

40. Yuzaki, M.; Forrest, D.; Verselis, L.M.; Sun, S.C.; Curran, T.; Connor, J.A. Functional NMDA receptors are transiently active and support the survival of Purkinje cells in culture. *J. Neurosci.* **1996**, *16*, 4651–4661.
41. Balazs, R.; Jorgensen, O.S.; Hack, N. N-Methyl-D-aspartate promotes the survival of cerebellar granule cells in culture. *Neuroscience* **1988**, *27*, 437–451.
42. Ortega, F.; Perez-Sen, R.; Morente, V.; Delicado, E.G.; Miras-Portugal, M.T. P2X7, NMDA and BDNF receptors converge on GSK3 phosphorylation and cooperate to promote survival in cerebellar granule neurons. *Cell. Mol. Life Sci.* **2010**, *67*, 1723–1733.
43. Kadotani, H.; Hirano, T.; Masugi, M.; Nakamura, K.; Nakao, K.; Katsuki, M.; Nakanishi, S. Motor discoordination results from combined gene disruption of the NMDA receptor NR2A and NR2C subunits, but not from single disruption of the NR2A or NR2C subunit. *J. Neurosci.* **1996**, *16*, 7859–7867.
44. Marmolino, D.; Manto, M. Past, present and future therapeutics for cerebellar ataxias. *Curr. Neuropharmacol.* **2010**, *8*, 41–61.
45. Bormann, J. Memantine is a potent blocker of N-methyl-D-aspartate (NMDA) receptor channels. *Eur. J. Pharmacol.* **1989**, *166*, 591–592.
46. Strupp, M.; Brandt, T. Current treatment of vestibular, ocular motor disorders and nystagmus. *Ther. Adv. Neurol. Disord.* **2009**, *2*, 223–239.
47. Yoshida, T.; Katoh, A.; Ohtsuki, G.; Mishina, M.; Hirano, T. Oscillating Purkinje neuron activity causing involuntary eye movement in a mutant mouse deficient in the glutamate receptor delta2 subunit. *J. Neurosci.* **2004**, *24*, 2440–2448.
48. Faulstich, M.; van Alphen, A.M.; Luo, C.; du Lac, S.; De Zeeuw, C.I. Oculomotor plasticity during vestibular compensation does not depend on cerebellar LTD. *J. Neurophysiol.* **2006**, *96*, 1187–1195.
49. Gordon, J.W.; Uehlinger, J.; Dayani, N.; Talansky, B.E.; Gordon, M.; Rudomen, G.S.; Neumann, P.E. Analysis of the hotfoot (ho) locus by creation of an insertional mutation in a transgenic mouse. *Dev. Biol.* **1990**, *137*, 349–358.
50. Kashiwabuchi, N.; Ikeda, K.; Araki, K.; Hirano, T.; Shibuki, K.; Takayama, C.; Inoue, Y.; Kutsuwada, T.; Yagi, T.; Kang, Y.; *et al.* Impairment of motor coordination, Purkinje cell synapse formation, and cerebellar long-term depression in GluR delta 2 mutant mice. *Cell* **1995**, *81*, 245–252.
51. Wilson, D.B. Brain abnormalities in the lurcher (Lc) mutant mouse. *Experientia* **1975**, *31*, 220–221.
52. Nishiyama, J.; Matsuda, K.; Kakegawa, W.; Yamada, N.; Motohashi, J.; Mizushima, N.; Yuzaki, M. Reevaluation of neurodegeneration in lurcher mice: Constitutive ion fluxes cause cell death with, not by, autophagy. *J. Neurosci.* **2010**, *30*, 2177–2187.
53. Cendelin, J.; Tuma, J.; Korelusova, I.; Vozeh, F. The effect of genetic background on behavioral manifestation of Grid2(Lc) mutation. *Behav. Brain Res.* **2014**, *271*, 218–227.
54. Schwartz, E.J.; Rothman, J.S.; Dugue, G.P.; Diana, M.; Rousseau, C.; Silver, R.A.; Dieudonne, S. NMDA receptors with incomplete Mg(2)(+) block enable low-frequency transmission through the cerebellar cortex. *J. Neurosci.* **2012**, *32*, 6878–6893.
55. Hepp, R.; Hay, Y.A.; Aguado, C.; Lujan, R.; Dauphinot, L.; Potier, M.C.; Nomura, S.; Poirel, O.; El Mestikawy, S.; Lambolez, B.; *et al.* Glutamate receptors of the delta family are widely expressed in the adult brain. *Brain Struct. Funct.* **2014**, doi:10.1007/s00429-014-0827-4.

56. Glitsch, M.D. Calcium influx through N-methyl-D-aspartate receptors triggers GABA release at interneuron-Purkinje cell synapse in rat cerebellum. *Neuroscience* **2008**, *151*, 403–409.
57. Liu, S.J. Biphasic modulation of GABA release from stellate cells by glutamatergic receptor subtypes. *J. Neurophysiol.* **2007**, *98*, 550–556.
58. Duguid, I.C.; Smart, T.G. Retrograde activation of presynaptic NMDA receptors enhances GABA release at cerebellar interneuron-Purkinje cell synapses. *Nat. Neurosci.* **2004**, *7*, 525–533.
59. Hirano, T.; Watanabe, D.; Kawaguchi, S.Y.; Pastan, I.; Nakanishi, S. Roles of inhibitory interneurons in the cerebellar cortex. *Ann. N. Y. Acad. Sci.* **2002**, *978*, 405–412.
60. Whittingham, D.G. Fertilization of mouse eggs *in vitro*. *Nature* **1968**, *220*, 592–593.
61. Tabata, T.; Sawada, S.; Araki, K.; Bono, Y.; Furuya, S.; Kano, M. A reliable method for culture of dissociated mouse cerebellar cells enriched for Purkinje neurons. *J. Neurosci. Methods* **2000**, *104*, 45–53.

心筋症のマウスモデル

――拡張型心筋症マウスモデルの心機能解析と遺伝子解析

Mouse models for cardiomyopathy

――Cardiac function and genetic analyses of a mouse model for dilated cardiomyopathy

鈴木　治(写真)　松田潤一郎

Osamu SUZUKI and Junichiro MATSUDA

(独)医薬基盤研究所疾患モデル小動物研究室

◎心筋症は，心筋の構造異常により心臓の機能低下をきたし心不全を呈する疾患の総称である．とくに重篤例では心臓移植が唯一の治療法となる深刻な病気であり，病態解明や治療法開発が求められている．これまでに，分子遺伝学的解析により多くの原因遺伝子が同定され，自然発症マウスモデルの探索に加え，遺伝学的知見をもとにした遺伝子改変技術により多数のマウスモデルがつくられてきた．本稿では，さまざまな遺伝子変異により生じる心筋症に対応したマウスモデルの一覧を示すとともに，著者らが独自に開発した拡張型心筋症モデルマウスが，発症率100%であり，ヒトの拡張型心筋症の多くの症状を呈し，あらたな視点からの病態解明に役立ち，さらに治療法開発にも有効に利用されていることを紹介する．

Key word　心筋症，病態モデル動物，遺伝子改変マウス，種差，遺伝子型判定法

心筋症は，心筋の構造異常により心臓の機能低下をきたし心不全を呈する疾患の総称であり，①肥大型心筋症(hypertrophic cardiomyopathy：HCM)，②拡張型心筋症(dilated cardiomyopathy：DCM)，③拘束型心筋症(restrictive cardiomyopathy：RCM)，④不整脈源性右室心筋症(arrhythmogenic right ventricular cardiomyopathy：ARVC)，などに分類されている．従来から特発性(原因不明)の心筋症として多くが難病に指定されている．現在では家系内での発症が認められるものを中心に分子遺伝学的解析が進み，原因遺伝子が同定されつつある[1]．

しかし，原因遺伝子が同定されても，すぐには治療法開発に結びつかないのが現状である．治療法開発にはその病態を反映する適切な病態モデル動物の開発・利用が必須である．あらたな治療薬開発や治療法開発には，遺伝子改変が比較的容易に行え，均一な遺伝的バックグラウンドをもち，繁殖も容易で多数の個体を実験室レベルで使用可能なマウスモデルが非常に重要である．

サイドメモ　遺伝子改変動物の遺伝子型

いわゆる遺伝子導入マウスの場合，遺伝子導入アレルには対応する対立遺伝子が存在しないため，正常アレルと遺伝子導入アレルをひとつずつもつ個体はヘテロ型(heterozygous)ではなくヘミ型(hemizygous)とよぶ．一方，ノックアウトマウスでは破壊された遺伝子座(ノックアウトアレル)はあらたな対立遺伝子が生成されたと解釈されるようで，正常アレルとノックアウトアレルをもつ個体はヘテロ型とよぶ．ただし，日常会話ではどちらの場合でもヘテロ型とよばれることが多いようである．ちなみに日常会話的といえば，核酸の5′や3′末端のことを5ダッシュ末端，3ダッシュ末端とよぶことが多いが，英語では5-prime endや3-prime endとよぶ(よって本来は，「'(apostrophe)」ではなく「′(prime)」を使うべきだが，入力の容易さから「'」での代用も多い)．要注意である．

表 1　遺伝性心筋症のおもな原因遺伝子とマウスモデル(文献[2]を改変)

遺伝子記号	遺伝子名	病型	マウスモデル
MYH7	myosin, heavy chain 7, cardiac muscle, beta	HCM, DCM	KO(no phenotype)
MYBPC3	myosin binding protein C, cardiac	HCM, DCM	KO, KI
TNNT2	troponin T type 2(cardiac)	HCM, DCM, RCM	KO(Embryonic lethal), KI, Tg
TNNI3	troponin I type 3(cardiac)	HCM, DCM, RCM	KO(Early death), Tg
TPM1	tropomyosin 1(alpha)	HCM, DCM	KO(Embryonic lethal), Tg
ACTC1	actin, alpha, cardiac muscle 1	HCM, DCM	KO(Embryonic/postnatal lethal), Tg
CSRP3	cysteine and glycine-rich protein 3 (cardiac LIM protein)	HCM, DCM	KO
LAMP2	lysosomal-associated membrane protein 2	HCM, DCM, Danon 病	KO
PLN	phospholamban	HCM, DCM	KO(No phenotype), Tg
DES	desmin	HCM, DCM	KO, Tg
ACTN2	actinin, alpha 2	HCM, DCM	—
VCL	vinculin	HCM, DCM	KO, KI
ANKRD1	ankyrin repeat domain 1(cardiac muscle)	DCM	KO(No phenotype)
MYL2	myosin, light chain 2, regulatory, cardiac, slow	HCM	KO(Embryonic lethal)
MYL3	myosin, light chain 3, alkali ; ventricular, skeletal, slow	HCM	—
PRKAG2	protein kinase, AMP-activated, gamma 2 non-catalytic subunit	HCM	Tg
GLA	galactosidase, alpha	HCM, Fabry 病	KO, KO/Tg
TTN	titin	DCM, HCM	KO/KI(Embryonic lethal)
DMD	dystrophin	DCM, Becker 病	KO, Spontaneous mutant
SGCD	sarcoglycan, delta	DCM	KO
LMNA	lamin A/C	DCM	KO, KI
RBM20	RNA binding motif protein 20	DCM	KO
TMPO	thymopoietin	DCM	KO
TCAP	titin-cap	DCM	KO
BAG3	BCL2-associated athanogene 3	DCM	KO(Postnatal lethal)
LDB3	LIM domain binding 3	DCM	KO, Tg
PKP2	plakophilin 2	ARVC	KO(Embryonic lethal)
DSP	desmoplakin	ARVC	Tg/KO

KO : gene knockout, KI : gene knockin, Tg : transgenic.

表 1 に示すように，ヒトで同定された遺伝子[2]に変異をもつマウスモデルが多数作製されており，病態発症の詳細なメカニズム解明に利用されている．しかし表でも明らかなように，遺伝子をノックアウトしたマウスモデルがヒトと同様の症状をかならずしも示すとは限らないこともあり，より適切なヒトの心筋症モデル動物の開発が期待されている．

本稿では，著者らが開発した拡張型心筋症マウスモデル(4C30 マウス[3])の有用性と，その解析に用いた技術について概説する．

拡張型心筋症モデルマウス(4C30マウス)

4C30 マウスは，シアル酸転移酵素 Galβ1,3GalNAc α2,3-sialyltransferase Ⅱ (ST3GalⅡ)[4](後述)を全身で強制発現させた遺伝子導入マウスの

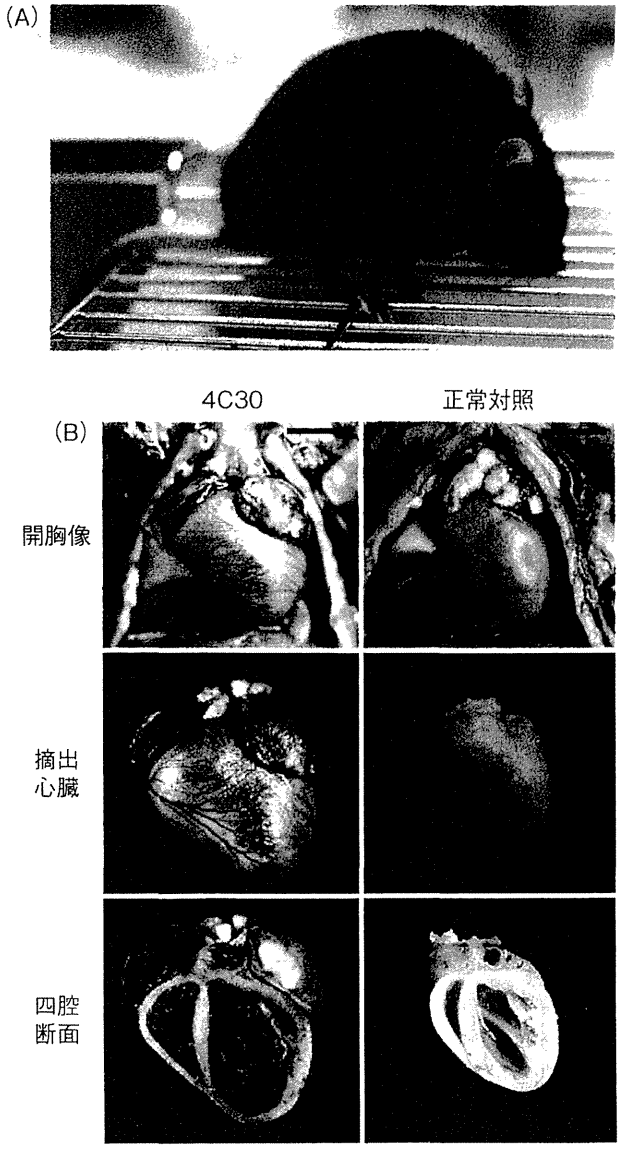

図 1　4C30マウスの様子[3]
A：全身像(末期)．B：拡張固定した心臓の様子(開胸像の Bar＝5 mm)．

ラインのひとつで，ホモ型特異的に平均7カ月で100%拡張型心筋症を発症して死亡する[3]．一方，ヘミ型個体(「サイドメモ」参照)や野生型では，1年以上生存する．体重ははじめは野生型と同様に増加していくが，あるとき急にやせてきて死に至る．末期(図 1-A)には，ガリガリにやせ，巨大化した心臓が肺を圧迫するため重度の呼吸障害が生じ，胸郭を広げて呼吸を確保するためか，背中を丸めてカエルのような姿勢をとる．その後の死亡は強度の削痩(るいそう)と呼吸不全によると考えられる．

10%中性ホルマリンとカルノア液を7：3で混合した液による拡張固定後の胸腔内の心臓をみると，発症例(4C30)は正常対照(C57BL/6NCr)に比べ心臓全体が著しく大きく，胸腔内を大きく占めていた(図 1-B 上段)．図 1-B 中段は摘出心の様子で，発症例では左右の心耳が双方とも著しく大きい．図 1-B 下段は心臓の四腔断面の写真で，発症例では対照例に比べ四腔とも拡大し，心房・心室の壁や中隔がすべて菲薄化するという典型的な拡張型心筋症を呈していた．4C30 では筋傷害の指標である血中 creatine phosphokinase や lactate dehydrogenase の上昇に加え[3]，心筋障害特異的な指標である血中 cardiac troponin I (cTn I)も有意に増加しており[5]，4C30 マウスはヒト拡張型心筋症の病態をよく模倣した有用なモデルであると思われる．

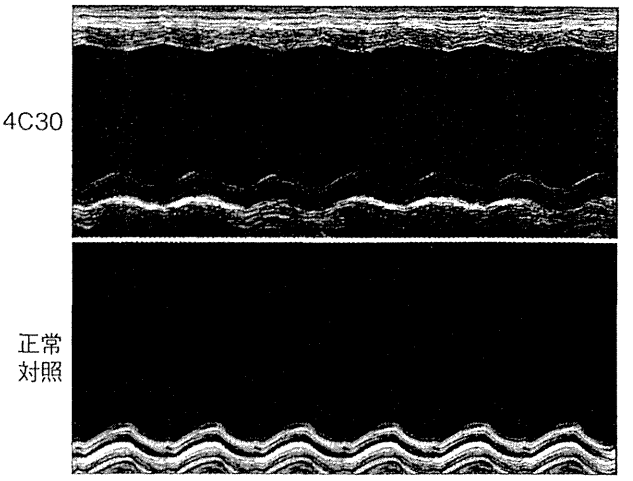

図 2　心エコー像の例(左室のMモード)
この例(15 週齢雄)では FS%は 4C30 で 15，正常対照(C57BL/6NCr)で 40 である．

4C30 は心機能の点でも心筋症を呈していることが確認されている．実験動物を用いた心機能解析では，ヒトとの種差を配慮する必要がある[6]．とくにマウスの心臓はサイズが小さいうえ，心拍数が非常に高いため(毎分300～700回)，超音波診断装置などはマウスに特化したものを用いたほうがよい．また，マウスの系統差も無視できない．たとえば，心エコーでの左室内径短縮率(FS%)は C57BL/6 マウスで 41±6[7]，ICR マウスで 36±4[8]との報告がある．実際，FS%は正常対照マウスでは 30～50 であるが，4C30 マウスでは 15～30 と低値であった(図 2)．このように，心収縮機能低下の出現という点でも 4C30 マウスは心筋症モデルとして有用である．

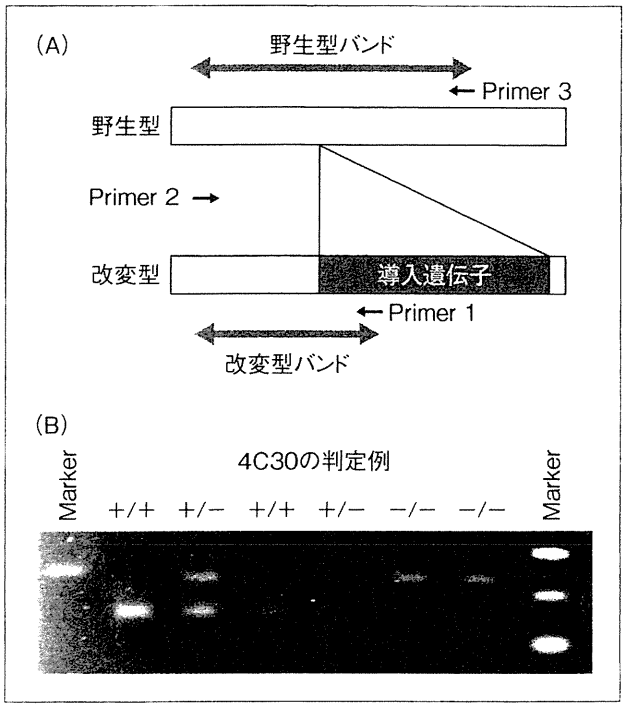

図 3 Flanking primerによるgenotyping PCR[15]
A：近傍プライマーの位置.
B：3つの近傍プライマーを同時に使用したPCRによる実際の遺伝子型判定例. ＋：Tgアリル, −：野生型アリル.

4C30マウスに導入された酵素ST3Gal Ⅱは，糖脂質や糖蛋白質の糖鎖の末端グルコースにα-2,3位にシアル酸を結合させる酵素のひとつで，マウス心臓では幼若期に発現しているが，成体では発現していない[9]．一方，ヒト心臓ではマウスと異なり成体でもST3Gal Ⅱが発現している[10]．4C30マウスの心臓では導入酵素ST3Gal Ⅱが蛋白レベルで高発現しており，心臓蛋白質の糖鎖組成に変化がみられることをレクチン染色で確認した[3]．また，4C30心臓でcalreticulinやcalnexinの蛋白質量の増加が観察されたことから，4C30マウスの心筋症発症の機序として以下を想定している．

導入したシアル酸転移酵素によりさまざまな蛋白質の糖鎖が変化し，それが小胞体(筋では筋小胞体)の蛋白質品質管理機構(endoplasmic reticulum quality control：ERQC)[11]を乱し，ERQCの中心的役割を担うcalreticulinやcalnexinの増加が起こり，一方，これらの蛋白質はカルシウム(Ca)結合能をもつことから，これら蛋白質の増加がCa代謝異常を惹起させることによって心筋の収縮障害が生じるのではないか，と推察している．とくにcalreticulinの増加は，心停止を引き起こすことから[12]，ERQCを介した糖鎖修飾の変化と心機能との関連性を示唆する知見といえる．また，Dystroglycan複合体の異常もみられ[5]，この点でもCa代謝異常の関与が強く示唆されている．

ST3Gal Ⅱの異常によるヒト拡張型心筋症の症例は報告されていないものの，ヒト心筋症においてもシアル酸転移酵素の発現量が増加しており[13]，また，一般に心筋症は原因によらず最終的には似たような病態・経過をたどるともいわれている．4C30マウスは上記のようにヒト拡張型心筋症の病態をよく模倣しており，病態解析や治療法開発用の拡張型心筋症モデルとして非常に有用であると思われる．これまでに伸展刺激感受性イオンチャネル(TRPV2)を標的とした心筋症治療法の開発[5]や，心機能マーカーである血中atrial natriuretic peptide(ANP)のアッセイ系開発[14]に4C30マウスが活用された．今後の活用にも期待したい．

ゲノム解析

遺伝子導入マウスでは，導入遺伝子のゲノム内挿入位置やコピー数が導入遺伝子の発現に影響する．4C30マウスの心筋症症状はホモ型個体に特異的なことから，導入遺伝子の発現量の影響か，導入遺伝子のゲノム内挿入による既存配列破壊のホモ化によって内因性遺伝子がノックアウトされた可能性が考えられた．そこで，導入遺伝子の近傍ゲノム配列をゲノムウォーキングにより決定し，その配列をゲノムデータベースで検索してゲノム上の位置を特定したところ[15]，δサルコグリカン(SGCD)遺伝子の上流領域であった．SGCDの欠損は心筋症になることから[16]，導入遺伝子挿入によるSGCDの発現抑制の可能性が示唆されたが，SGCDの心臓内発現量は正常だったため，現時点では導入遺伝子の発現量が発症に重要であると考えている．

遺伝子導入動物の導入遺伝子の遺伝子型判定法(zygosity check，ホモ型・ヘミ型判定法)には多々あるが[17]，近傍ゲノム配列情報が必要なものの，定性的な判断が可能で，導入遺伝子の有無だけでなく遺伝子型も同時に判定できる“近傍プラ

イマーによるPCR”が実用的である．幸い，4C30マウスではゲノムウォーキングにより近傍ゲノム配列が得られていたので，この方法で遺伝子型を明確に判別することができる(図3)[15]．

おわりに

本稿でおもに取りあげた拡張型心筋症は，一般的には予後の悪い疾患で，最終的には心臓移植の適応となる難病である．実際に，国内の心臓移植希望者の8割が本症の罹患者といわれており，小さな子どもが海外で心臓移植を受ける例も多く報道されている．一方，治療薬や治療法の開発が進んでおり，進行を遅らせるなど予後の改善に大きく貢献している．今後，先端的な治療薬などの開発には，高度で実験的な治療を生きたモデル動物を用いて行うことが重要となり，そのためには臨床予測性が高く，ヒトにより近い病態を示すモデルマウスの利用がいっそう求められる．

今回紹介した新規の拡張型心筋症モデルマウスが有効に利用され，心筋症の解明や治療法の開発に貢献し，難病の患者にすこしでも役立つことを期待する．なお，4C30マウスは，(独)医薬基盤研究所実験動物研究資源バンク(http://animal.nibio.go.jp/)から入手可能である．

文献/URL

1) Online Mendelian Inheritance in Man.(http://omim.org/)
2) 森崎裕子：医学のあゆみ，**250**：365-370，2014.
3) Suzuki, O. et al.：*Proc. Jpn. Acad. Ser. B Phys. Biol. Sci.*, **87**：550-562, 2011.
4) Lee, Y. C. et al.：*J. Biol. Chem.*, **269**：10028-10033, 1994.
5) Iwata, Y. et al.：*Cardiovasc. Res.*, **99**：760-8, 2013.
6) 菅野　茂・他：基礎と臨床のための動物の心電図・心エコー・血圧・病理学検査．アドスリー，2013.
7) Tanaka, N. et al.：*Circulation*, **94**：1109-1117, 1996.
8) Kudej, R. K. et al.：*J. Mol. Cell. Cardiol.*, **29**：2735-2746, 1997.
9) Kono, M. et al.：*Glycobiology*, **7**：469-479, 1997.
10) Kim, Y. J. et al.：*Biochem. Biophys. Res. Commun.*, **228**：324-327, 1996.
11) Kopito, R. R.：*Cell*, **88**：427-430, 1997.
12) Nakamura, K. et al.：*J. Clin. Invest.*, **107**：1245-1253, 2001.
13) Hwang, J. J. et al.：*Physiol. Genomics*, **10**：31-44, 2002.
14) Nagai, C. and Minamino, N.：*Anal. Biochem.*, **461**：10-16, 2014.
15) Noguchi, A. et al.：*Exp. Anim.*, **53**：103-111, 2004.
16) Sakamoto, A. et al.：*Proc. Natl. Acad. Sci. USA*, **94**：13873-13878, 1997.
17) Behringer, R. et al.：Manipulating the Mouse Embryo：A Laboratory Manual, 4th ed. Cold Spring Harbor, New York. 2014, pp.551-570.

*　　*　　*